

ARTICLE OPEN



Nanowire-assisted freestanding liquid metal thin-film patterns for highly stretchable electrodes on 3D surfaces

Minwoo Kim^{1,5}, Chulmin Cho^{1,2,5}, Wooseop Shin¹, Jung Jae Park¹, Jaewon Kim¹, Phillip Won³, Carmel Majidi³✉ and Seung Hwan Ko^{1,4}

Stretchable electronics is playing an integral role in fields such as wearable electronics and soft robots. Among soft conductive materials, liquid metal is drawing intense attention as an electrode material due to its liquid nature at room temperature. However, the merits of liquid metal conductor are limited by the presence of substrates or enclosed microchannels from physical disturbances by the underlying substrate when applying it to 3D surface and modifying complex circuit. To overcome this limitation, we develop freestanding patterned liquid metal thin-film conductor (FS-Galn). FS-Galn was achieved by introducing metal nanowires to liquid metal and subsequent sequential selective laser processing and etching of directly patterned traces. FS-Galn can be applied directly to nonflat surface without substrates. When incorporated into electrical circuits, FS-Galn shows high electrical conductivity, stretchability, and stability. The concept of freestanding liquid metal can open a functionality to the conventional liquid metal electronics.

npj Flexible Electronics (2022)6:99; <https://doi.org/10.1038/s41528-022-00232-1>

INTRODUCTION

Stretchable and soft electronics are drawing attention in various emerging fields, such as wearable electronics^{1–4}, bio-medical devices⁵, flexible optical devices⁶, and soft robots^{7,8}. Within these fields, the stretchable conductive material represents an important and fundamental component, and remains the focus of intense research. Studies regarding stretchable conductor have been widely reported as follow; conductive elastomer^{9–11}, metal nanowire^{9,12}, and deterministically patterned metal thin-film conductor¹. While highly promising for many applications, these approaches to stretchable circuit functionality have limitations that can interfere with their use in certain cases. For example, conductive elastomer and metal nanowire conductor can be limited in their functionality due to some combination of low volumetric conductivity, high electromechanical coupling, or poor elasticity. Likewise, deterministic architectures typically require advanced manufacturing techniques for patterning of wavy or serpentine traces of thin-film conductors. At the same time, they have limited stretchability and low areal density due to non-straight pattern.

Stretchable conductors composed of liquid metal (LM) at room temperature have been widely reported in order to address the aforementioned limitations¹³. LM has appropriate properties for stretchable conductors such as high conductivity, extreme stretchability, patternability, and compliance that stems from inherent liquid-nature^{14–16}. LM-based conductors have resolved the necessary capabilities for stretchable conductors. For instance, Tavakoli et al. introduced 3D hydrographic printing of inkjet printed AgNP-EGaln on a tattoo paper that could be directly transferred to a highly curved surface¹⁴. Liu et al. presented biphasic gallium-indium fabricated by a heated furnace at 900 °C that had stretchability over 1200% with stable electromechanical property¹⁵. Choi et al. has developed a fabrication method of 3-D

electronics based on pre-distorted pattern generation for precise patterning on complicated 3-D surfaces¹⁶. Lucy et al. has achieved high resolution of LM pattern by applying it on the pre-deposited gold¹⁷. Kim et al. has developed a stretchable printed circuit board platform by realizing universal leak-free liquid metal interconnection with AgNW and LM¹⁸.

Despite great researches that have been conducted so far, the merits of liquid metal conductors are still largely limited by the presence of a substrate or an enclosed microchannel. A circuit with a substrate inevitably suffers from an unsolvable dilemma that the substrate and the circuit always go in couples; the substrate below the fabricated circuit inevitably hinders movement, attachment, repair and modification of the patterned circuit restricting the applicability of it. For this reason, researchers are actively developing thin and compliant substrates to minimize the negative effects caused by the substrate^{12,19}. Nevertheless, the presence of substrate inevitably causes the aforementioned disturbances to the conductor, and it is impossible to completely exclude those problems without removing the substrate thoroughly. In order to overcome the limitations provoked by substrate and extend the applicability of stretchable conductor, an emergence of freestanding, or substrate-free conductor with superior electromechanical property is required.

Here, we introduce a freestanding patterned liquid metal thin-film conductor (FS-Galn) that is able to stand alone in substrate-free state and be directly applied to irregular surfaces. FS-Galn is fabricated by introducing metal nanowires to the liquid metal, and subsequent sequential selective laser processing and selective etching in maskless and room temperature condition. The laser-assisted fabrication facilitates ultrafast patterning (laser scanning speed of 100 mm s⁻¹) and rapid prototyping. When incorporated to electrical circuits, FS-Galn withstands extreme strain with a small change in resistance without encapsulation, forms stable

¹Applied Nano and Thermal Science Lab, Department of Mechanical Engineering, Seoul National University, Seoul, Gwanak-gu, Korea. ²Mechatronics Research, Samsung Electronics, Hwaseong-si, Gyeonggi-do, Korea. ³Soft Machines Lab, Department of Mechanical Engineering, Carnegie Mellon University, Pittsburgh, PA, USA. ⁴Institute of Advanced Machines and Design/Institute of Engineering Research, Seoul National University, Seoul, Korea. ⁵These authors contributed equally: Minwoo Kim, Chulmin Cho. ✉email: cmajidi@andrew.cmu.edu; maxko@snu.ac.kr

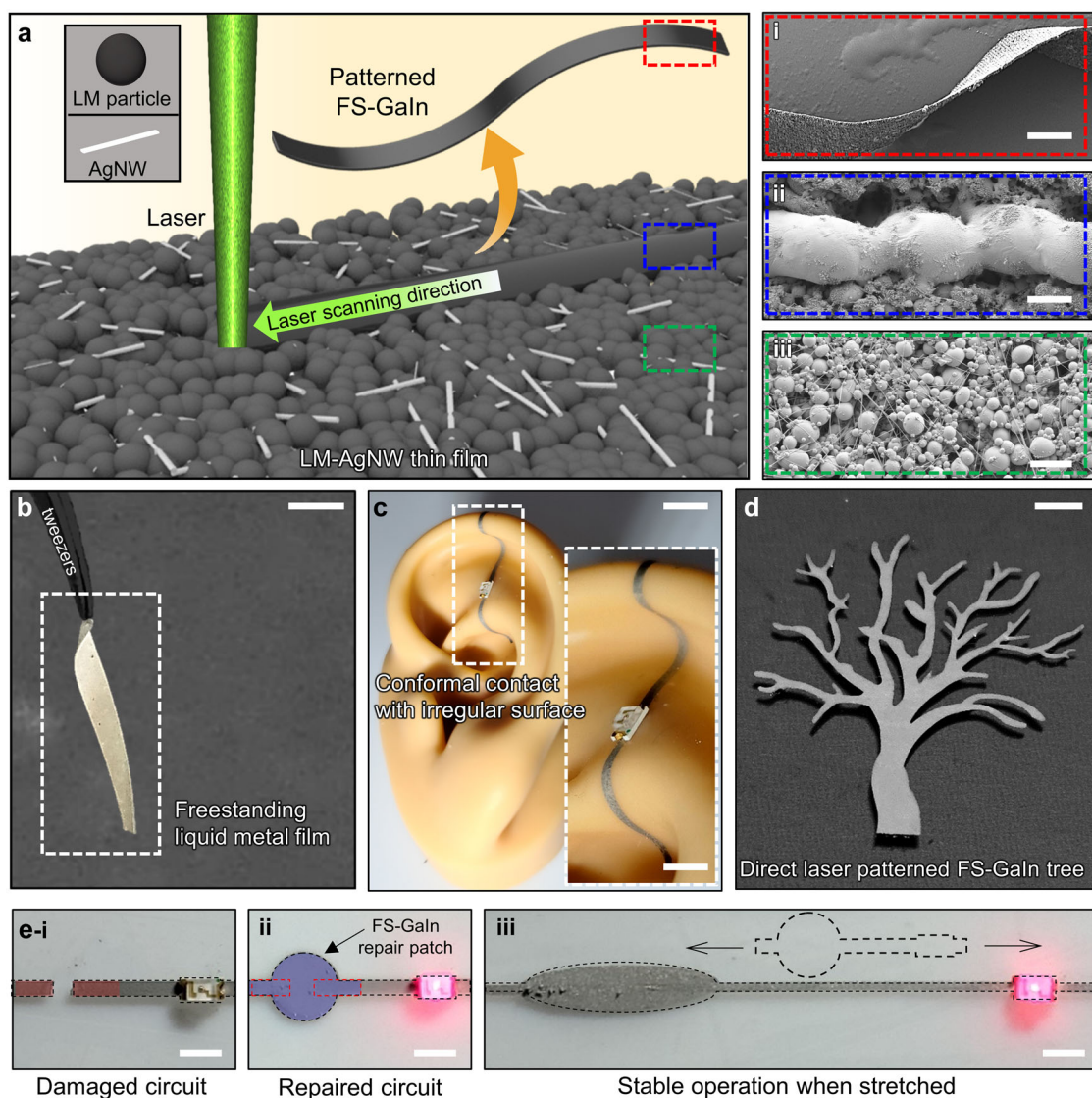


Fig. 1 Freestanding LM-AgNW thin-film conductor (FS-Galn). **a** Schematic illustration of the FS-Galn fabrication process (i) SEM of the FS-Galn. (ii, iii) SEM of the LM-AgNW thin-film after and before laser exposure, respectively. **b** The FS-Galn held by tweezers. **c** Conformal contact of the FS-Galn with a human ear model and a rigid component. **d** The tree-patterned FS-Galn. **e** In situ circuit reconnection with a FS-Galn repair patch and stretchability after reconnection. (i) A disconnected circuit with LED off. (ii) The reconnected circuit by the FS-Galn repair patch with LED on. (iii) Stable operation of the repaired circuit under stretched condition with the well-operating LED and the repair patch. Scale bars: 200 μm (a-i), 6 μm (a-ii, iii), 2 mm (b), 10 mm (c), 4 mm (c inset), 3 mm (d, e).

electrical contact with a rigid component with no post-processing, and is capable of making conformal contact with uneven 3-D surfaces. A modified circuit by FS-Galn also shows great stability. FS-Galn is an exceptional metal-based hyper-stretchable thin-film conductor that can be applied to bumpy 3-D surfaces or utilized for in situ circuit modification, extending the field of soft and stretchable electronics with the feature of substrate-free thin-film liquid metal conductor.

RESULTS

Introduction of FS-Galn

FS-Galn is fabricated by direct laser patterning of a vacuum-filtrated LM-Ag nanowire (LM-AgNW) thin-film with continuous visible laser and subsequent selective etching (Fig. 1a). A scanning electron microscope (SEM) image in Fig. 1a-i shows the FS-Galn (Pattern resolution in Supplementary Fig. 1). It possesses high electrical conductivity of $5.79 \times 10^5 \text{ S m}^{-1}$ with thickness of

around 12 μm (Supplementary Fig. 2). SEM images in Fig. 1a-ii, a-iii demonstrate the thin-film after and before laser exposure, respectively. Exposing the laser to the thin-film induces multi-phase sintering of LM and AgNW, which eventually generates FS-Galn after an etching process. Figure 1b demonstrates an image of FS-Galn that is raised by tweezers. Since FS-Galn can exist without any substrate, it is possible to be raised solely. Moreover, as shown in Fig. 1c, it can be applied to an irregular 3-D surface such as an ear model or attached to a rigid component to form a stable connection with mild pressure¹⁵ (Fig. 1c inset). Figure 1d demonstrates a tree-patterned FS-Galn by direct laser writing with computer-aided design (Supplementary Fig. 3) and subsequent selective etching. FS-Galn's property of substrate-free has great potential by granting a circuit an ability of in situ modification. As shown in Fig. 1e-i, an FS-Galn with an LED is off due to the disconnection of the circuit. An FS-Galn repair patch is attached to the disconnected area with gentle pressure, and the LED is turned on (Fig. 1e-ii). Moreover, the repaired circuit with the LED and the

repair patch can be elongated without any disconnection indicated by the brightly shining LED (Fig. 1e-iii and Video S1).

FS-GaIn fabrication principle and process

Figure 2a shows the laser processed LM-AgNW thin-film in a cross-sectional view (SEM images in Supplementary Fig. 4). The apricot arrow in Fig. 2a-i exhibits the region where laser is scanned. The laser process allows localized heat treatment to the film inducing multiphase sintering of LM and AgNW, and further oxidation of LM surface^{15,20} (Blue box in Fig. 2a-i). In previous studies, laser sintering is generally defined as a junction connection between Ag nanowires due to the heat concentration by a plasmonic effect²¹ or an aggregation of LM particles due to a rupture of the gallium oxide shell, respectively²⁰. However, in this research, these two processes happen simultaneously due to the coexistence of LM particles and AgNWs in the laser-scanned region. This phenomenon is defined as multiphase sintering in this research article. As the laser is exposed to the composite film of LM and AgNW, LM undergoes small explosion and the liquid core covers the AgNW due to the capillary force and the metallic binding force between them²², where other LM coalesces together. These results of coalescence between the two with enhanced interaction can be seen as gross coalescing in Fig. 2a-ii and Supplementary Fig. 5, and as AgNW wetting by LM in Fig. 2a-iii¹⁴. The synergistic effect of multiphase sintering realizes the fabrication of FS-GaIn, whereas sintering of either LM or AgNW solely does not (Supplementary Fig. 6 in Supporting Information). The multiphase sintering grants more etch-resistivity to the sintered region (Fig. 2a-ii, iii) than the non-sintered region (Fig. 2a-iv) (See Supplementary Note 1 in Supporting information for further discussion)²³. This difference allows the non-sintered portion of the film to be etched away using a 0.2M aqueous solution of sodium hydroxide (NaOH). Not only that, in order to create FS-GaIn, the localized heat from laser should only affect the surface of the film so that the film is divided into the laser-induced sintered region (Blue box in Fig. 2a-i) and non-sintered region (Green box in Fig. 2a-i) in-depth as well as in-plane. This in-depth division is realized by fast laser scanning speed (100 mm s^{-1}). When the etching process is conducted, the multiphase sintered region (Blue box in Fig. 2a-i) becomes FS-GaIn.

Figure 2b demonstrates the steps where laser sintering and solvent etching is used to create patterned FS-GaIn in perspective view, cross-section view, and real image, respectively (Video S2 for the fabrication of FS-GaIn). First, an LM-AgNW thin-film is synthesized using the vacuum filtration process (described in Supplementary Fig. 8 and Supplementary Note 2 of the Supporting Information and Methods section). Then, the desired pattern is drawn using CAD-assisted direct laser writing in maskless and room temperature condition (Fig. 2b-i). Next, an etchant (0.2M NaOH) is applied to remove the non-sintered region. In this step, a separation between the sintered region (Blue box and region in Fig. 2a, b-ii, respectively) and the non-sintered region (Green box and region in Fig. 2a, b-ii, respectively) occurs. Finally, only the sintered FS-GaIn remains as shown in Fig. 2b-iii.

Electromechanical characteristic of FS-GaIn

We have measured the electromechanical properties of FS-GaIn in order to investigate its applicability as a stretchable thin-film electrode. Most previous LM studies required encapsulation of the liquid metal with elastomer in order to prevent leaking, smearing, or marking of the fluid and maintain material integrity. In this study, we placed the patterned film on VHB tape (3 M) but did not apply an encapsulating sealing layer. Figure 3a shows the electromechanical behavior from the pristine state to the most stretched state prior to failure. FS-GaIn endures up to 1358 % strain and a corresponding resistance change of about ten times its initial resistance value (i.e., $\Delta R/R_0 \sim 10$). While 1358 % was the

maximum measurement, most samples fractured at around 1000% strain (Supplementary Fig. 9 in Supporting Information). The value of maximum strain and the corresponding resistance change can be considered as remarkable compared to other thin-film conductor that researchers have studied, as shown in Fig. 3c. At relatively low-strains (100%), the gauge factor ($(\Delta R/R_0)/(\Delta L/L_0)$) is around 0.2 as shown in the Fig. 3a inset, well below that would be predicted by Pouillet's law for a stretchable conductor. This is comparable to other LM-based electrode that other researchers have previously shown^{15,24}. The repeatability of FS-GaIn is investigated through cyclic 100 % strain tests (Fig. 3b). Over 10,000 loading cycles, a stable resistance value is measured after initial loading cycle. The maximum resistance value relative to the initial resistance is sustained around 1.3 (i.e., $R/R_0 \sim 1.3$) with steady ups and downs corresponding to the applied strain. The stability of FS-GaIn presents it can be used for a strain sensor in wearable electronics as well as stretchable electrode. (Supplementary Fig. 10 in Supporting Information for FS-GaIn sensor.)

Figure 3d demonstrates SEM images of FS-GaIn in stretching condition in top view for both laser-treated side and not-treated side. The laser-treated side of FS-GaIn film is initially composed of agglomerations of LM-AgNW nanomaterials that are uniformly aligned along the laser scanning direction (Fig. 3d-i). At the same time, the laser-not-treated side is composed of multiphase sintered LM and AgNW though not forming an agglomeration (Fig. 3d-ii). According to the images in Fig. 3d-iii, d-iv, the agglomerations on laser-treated side and the sintered LMs and AgNWs on the other side are being stretched simultaneously allowing negligible resistance change.

The negligible resistance change with extreme stretchability can be understood by explaining three main factors. These three factors are surface reconciliation, wettability between LM and AgNW, and highly tortuous serpentine conductive path. FS-GaIn has a core-shell structure that consists of LM and AgNW core, and laser-induced beta gallium oxide shell. Before FS-GaIn is attached to an arbitrary substrate, it can maintain its structure while being held due to robust laser-induced beta gallium oxide shell. However, it does not possess stretchability because there is no place for liquid metal in the core to smear when the oxide shell ruptures. Therefore, FS-GaIn gains stretchability after it is attached to any arbitrary surface. (Supplementary Fig. 11 in Supporting Information) In this process, surface reconciliation becomes an important factor²⁵. When the substrate and FS-GaIn adhere to each other with high affinity, it possesses high stretchability and small gauge factor. As shown in Supplementary Fig. 12, the reconciliated surface between FS-GaIn and substrate can be thought as anchoring sites. When FS-GaIn and the substrate are stretched, the anchoring sites of FS-GaIn firmly adhere to the substrate which subsequently results in downward net-force for other parts of FS-GaIn. This causes continuous electrical path of FS-GaIn in the subsequent stretching resulting in ultra-high stretchability without electrical failure. Besides, the stretching out of FS-GaIn barely changes the end-to-end conductance due to the highly tortuous serpentine conductive path composed of LM particles whose length and cross-sectional area does not change much when stretched as depicted in Supplementary Fig. 13²⁶. This geometrical characteristic contributes to negligible resistance change. Moreover, the extreme stretchability of FS-GaIn is also intensified by the wettability between LM particles and AgNWs. When FS-GaIn is extremely stretched, the superior wettability between LM and AgNW induces a continuous and highly conductive electrical path, preventing the formation of electrically isolated liquid droplets that disconnects an electrical path^{14,15}. Both the structure and interaction between LM and AgNW realize extreme stretchability with negligible resistance change.

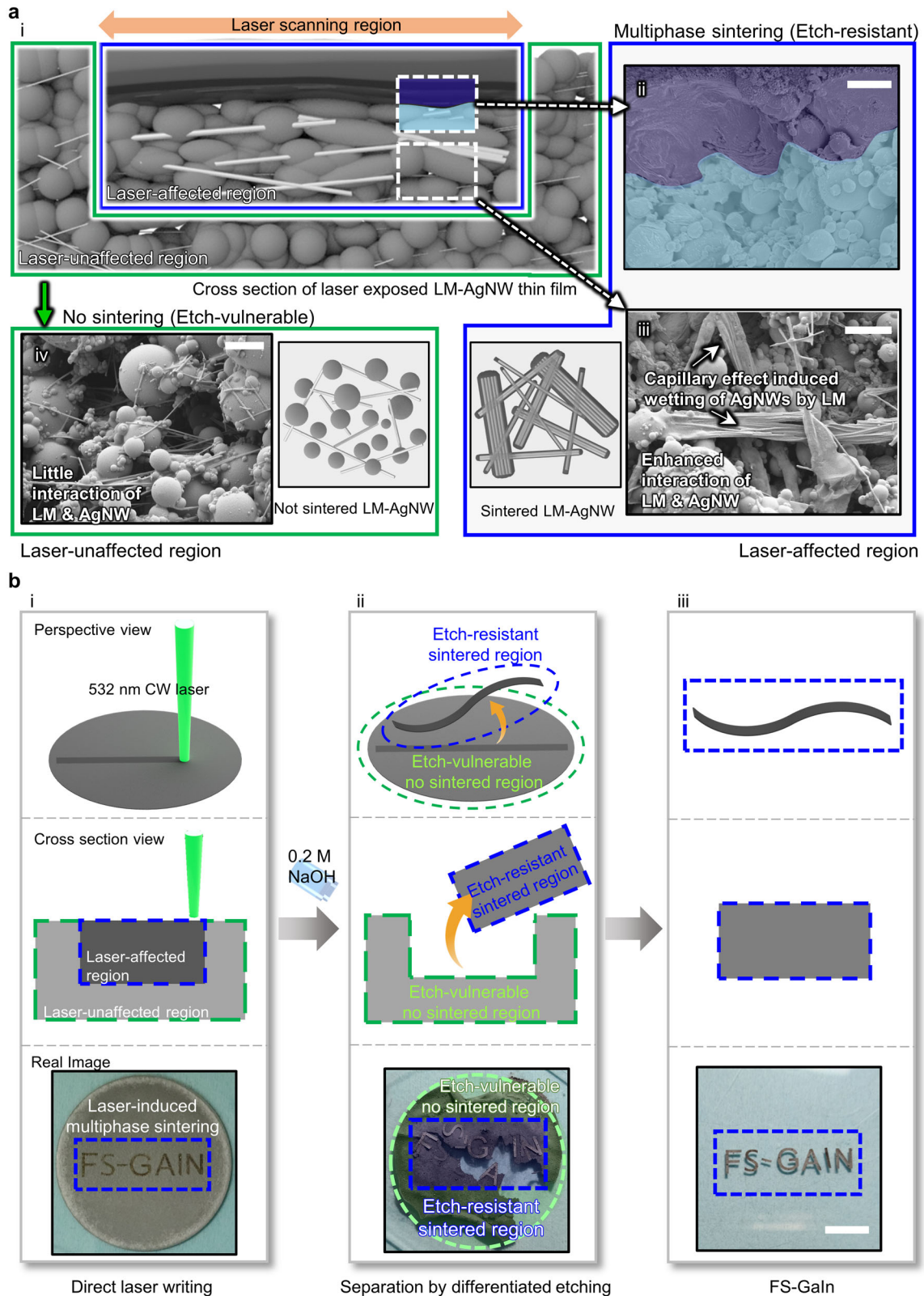


Fig. 2 FS-Galn fabrication principle and process. **a** (i) Schematic illustration of the laser-scanned LM-AgNW thin-film in cross-section view. The blue and green box represents laser scanned and non-scanned region, respectively. (ii) SEM image of the laser-scanned near-the-surface region as a cross-section view with pseudo-colors. (iii) SEM image of the laser-scanned deeper region and schematic illustration of multiphase sintered LM-AgNW. (iv) SEM image of the non-laser-scanned region and schematic illustration of not sintered LM-AgNW. **b** The fabrication process of FS-Galn in perspective view, cross-section view, and real image. (i) Direct laser writing on the LM-AgNW thin-film. (ii) FS-Galn separation by differentiated etching. (iii) The fabricated FS-Galn. Scale bars: 3 μm (**a**), 9 mm (**b**).

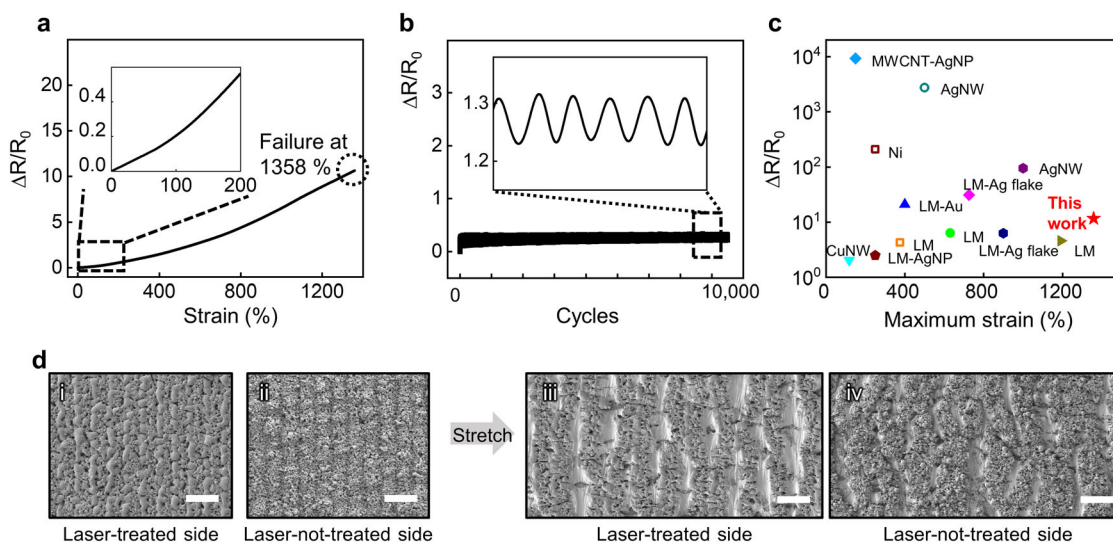


Fig. 3 Electromechanical characteristic of FS-GaN. **a** Relative change in electrical resistance of FS-GaN trace subjected to uniaxial strain with a displacement rate of 0.5 mm s^{-1} . **b** Relative change in resistance under cyclic loading from 0% to 100% strain up to 10,000 cycles. Inset: detailed electromechanical behavior near the end of the cyclic test. **c** Comparison of relative resistance change at maximum strain with other thin-film conductors: liquid metal^{15,19,29} (LM), liquid metal and Au³⁰ (LM-Au), liquid metal and Ag nanoparticles¹⁴ (LM-AgNP), liquid metal and Ag flakes^{24,31} (LM-Ag flake), multi-walled carbon nanotubes and Ag nanoparticles³² (MWCNT-AgNP), Ag nanowires^{33,34} (AgNW), Cu nanowires^{21,35} (CuNW, Ni). **d** SEM images of FS-GaN in stretching condition: (i) laser-treated side, (ii) laser not-treated side, and (iii), (iv) after stretched, respectively. Scale bars: $30 \mu\text{m}$ (**d**).

Applications of FS-GaN

FS-GaN has many advantages over conventional substrate-based stretchable thin-film conductors. For instance, it is not possible to modify or repair traditional printed circuits without replacing or soldering damaged material. Likewise, typical circuits require soldering or other forms of post processing in order to mount rigid components. In contrast, FS-GaN exhibits a substrate-free feature that allows for in situ circuit modification and repairs. It also possesses liquid-like property that enables an integration with rigid components without the need for a post-processing step¹⁵. Figure 4a compares the electromechanical response between a pristine FS-GaN circuit and a repaired one. In order to fabricate the repaired FS-GaN circuit, a pristine FS-GaN (Fig. 4a-i) is erased in the middle (Fig. 4a-ii). The erased FS-GaN is reconnected by simply placing a circle-patterned FS-GaN repair patch onto it with a gentle push to make electrical contact. (Fig. 4a-iii) This repaired circuit can be stretched up to nearly the same amount (1202%) compared to the pristine one (Fig. 4a). Furthermore, the gauge factor at 100% strain is also comparable to the pristine FS-GaN, 0.76 (Fig. 4a inset). It is confirmed that not only the pristine circuit, but also the repaired one can be used as a stable stretchable circuit.

FS-GaN's electromechanical behavior when connected with a rigid component is shown in Fig. 4b. The length of a rigid component—in this case a zero-ohm resistor—is about 3 mm, and the length of the FS-GaN traces on each side of it is 3 mm. The electrical contact becomes disconnected when the sample is stretched to about 30 mm. This suggests that the circuit fails when the FS-GaN electrodes (6 mm total) undergo over 500% strain, assuming that the length of the zero-ohm resistor (3 mm) remains fixed. This result shows that FS-GaN can operate firmly when connected to rigid components with having stable contact.

Figure 4c demonstrates the in situ circuit manipulation with FS-GaN. At first, FS-GaN is connected to an LED with stable electrical contact shown by the brightly illuminating LED. Then, a newly patterned FS-GaN circuit (blue color in Fig. 4c left bottom inset) is simply added above the original circuit (red color in Fig. 4c left bottom inset) extending from the circuit with one LED to the circuit with two LEDs (Fig. 4c-ii). Stable contact is easily made on

account of the FS-GaN's fluidity as shown in the SEM image²⁷ (Fig. 4c left bottom inset). Moreover, when the circuit is erased or worn out (Fig. 4c-iii), simply laying a newly made FS-GaN repair patch onto it can easily reconnect the circuit indicated by two bright LEDs (Fig. 4c-iv). The magnified view of the connection of the circuit can be seen in the right top inset in Fig. 4c with pseudo-colors.

There may be situations where conventional circuits cannot be installed due to many reasons, such as disturbance by an underlying substrate, a limitation in the pattern resolution, various physical obstacles, or inapplicability because of an irregular 3-D target surface. Among these restrictions, Fig. 4d demonstrates four representative circumstances where each circumstance is overcome owing to FS-GaN's properties of substrate-free feature, patternability, and shape-adaptability. In Fig. 4d-i, there is a cube-shaped obstacle in the way. By patterning the FS-GaN circuit with the shape of a detouring path, an LED can be lit. As shown in Fig. 4d-ii, two cube-shaped obstacles are closely spaced and allow for only a narrow path to connect the circuit (slightly over $100 \mu\text{m}$). A $100 \mu\text{m}$ thick FS-GaN is made and connected to an LED thanks to the high pattern resolution and substrate-free feature of FS-GaN. FS-GaN can also be folded at a right angle (90°) without any failure owing to its liquid-like deformability. FS-GaN is folded and conformally attached to a cube in Fig. 4d-iii. An illuminated LED in the figure indicates a stable and continuous folded electrical path. Figure 4d-iv demonstrates that FS-GaN is directly attached to a miniaturized mountain model with high curvature and rough surface presenting its shape-adaptability and substrate-free property.

DISCUSSION

In this work, we have introduced FS-GaN that has high electrical conductivity ($5.79 \times 10^5 \text{ S m}^{-1}$) with small resistance change over 1350% strain, cyclic stability over 10,000 cycles of 100% strain, and stable contact with a rigid component when stretched. The exceptional electromechanical property of FS-GaN stems from three major factors which are surface reconciliation, highly tortuous serpentine structure, and wettability between LM and

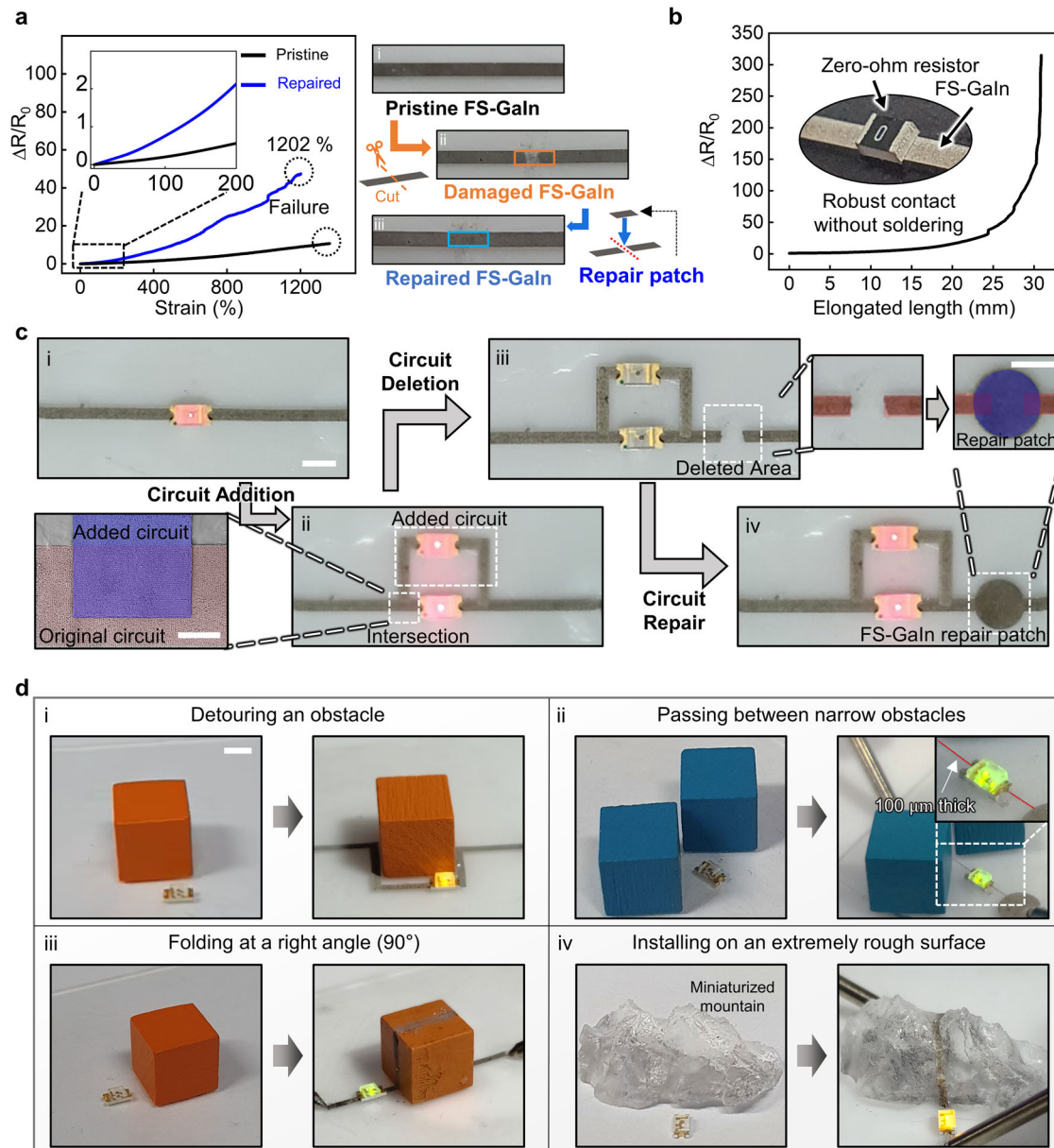


Fig. 4 Applications of FS-Galn. **a** Electromechanical behavior of the pristine and repaired FS-Galn circuit. (i) The pristine FS-Galn, (ii) The deliberately damaged FS-Galn. (iii) The repaired circuit by the FS-Galn repair patch. **b** Relative change in resistance as a function of the uniaxial tensile strain (0.5 mm s^{-1}) of the FS-Galn trace with a zero-ohm resistor. Inset: the digital image of the FS-Galn with a zero-ohm resistor. **c** Demonstration of the in situ circuit modification with FS-Galn. (i) A circuit with LED on. (ii) In situ circuit addition by placing a new FS-Galn circuit with another LED. Inset: the SEM image of the original circuit (red pseudo-color) and the newly added circuit (blue pseudo-color) (iii) A disconnected circuit with LEDs off. Inset: the digital image of the damaged area (red pseudo-color). (iv) Repaired circuit with the FS-Galn repair patch indicated by two bright LEDs. Inset: the digital image of the original circuit (red pseudo-color) and the newly added repair patch (blue pseudo-color). **d** FS-Galn's utility in various constrained situations: (a) detouring an obstacle, (b) passing between narrow obstacles, (c) folding at a right angle (90°), and (d) installing on an extremely rough surface of a miniaturized mountain. Scale bars: 3 mm (c, d), 300 μm (c left inset), 2 mm (c right inset).

AgNW. A circuit repaired by applying an FS-Galn patch also demonstrates stable contact and the ability to withstand over 1000% strain without electrical disconnection. The facile fabrication method of FS-Galn using a combination of direct laser writing and etching enables the rapid fabrication of appropriately patterned FS-Galn in maskless and room temperature condition. The fabrication of FS-Galn is realized by fully utilizing the differentiated etching behavior between multiphase sintered region and not sintered region. The features of FS-Galn also make it possible to perform in situ circuit modification, attachment to 3-D surfaces with sharp contours, and installation of a circuit in

constrained circumstances. It is expected that applying FS-Galn to wearable electronics, flexible optical devices, and soft robots will open up the next-generation stretchable electronics surmounting inevitable limitations with conventional thin-film conductors.

METHODS

Preparation of Ag nanowires

Ag nanowires were synthesized relatively long (100 μm or less in length with 1000:1 aspect ratio) using a modified polyol process.

For convenient synthesis, all reagents are blended into a triangular flask simultaneously as the one-pot process²⁸. In 50 ml of ethylene glycol (EG), 0.4 g of polyvinylpyrrolidone (Mw \approx 360,000) and 0.5 g of silver nitrate (AgNO₃) were successively dissolved using a magnetic stirrer. After all reagent chemicals were comprehensively dissolved, the magnetic stirrer was delicately removed from the mixture solution. Next, 800 μ L of copper(II) chloride dihydrate solution (CuCl₂·2H₂O, 3.3 mM dilution with EG) was swiftly injected into the mixture solution and then stirred moderately. Lastly, the triangular flask with the mixture solution was located in a 130 °C silicone oil bath for 3 h to grow Ag nanowires. After the desired growth was accomplished, the solution containing synthesized Ag nanowires was cleaned using acetone and ethanol with centrifugation of 3000 rpm for 10 min to eliminate the residual chemicals. The previous cleaning step was repeated three times. In the end, the prepared Ag nanowires were kept in ethanol for use.

Liquid metal particles

In this study, eutectic gallium-indium alloy (EGaln) was selected to be utilized among several room temperature liquid metals. Gallium (Ga, 99.99%) and indium ingot (In, 99.99%) were purchased from ROTOMETALS. 75.5 wt% of gallium (Ga) and 24.5 wt% of indium (In) were put together in a beaker and heated at 200 °C with 200 rpm of magnetic stirring for 24 h to make EGaln. After fabricating EGaln, a tip sonicator (UH-1200Z with Φ 13 mm probe, Fangke Technology (Shanghai) Co., LTD.) was used to break liquid metal into microparticles. The tip sonicator was operated for a total of 15 min (1 min operation, 1 minute rest, 8 times repetition, power setting with 95%) to sonicate 80 ml of ethanol and 8 ml of EGaln mixture in a beaker, where the beaker was immersed in an ice-water bath.

LM-AgNW thin-film transfer

The LM-AgNW thin-film with uniform thickness was fabricated by the vacuum filtration process. 2000 μ l of AgNW solution (density: 5.5 mg ml⁻¹), 500 μ l of liquid metal particle solution (density: 580 mg ml⁻¹) and 9 ml of ethanol were mixed in a 20 ml vial glass. Then, nylon and PTFE film were sequentially placed on the funnel. The mixed solution was used for vacuum filtration with enough amount of ethanol. The LM-AgNW thin-film on PTFE film was transferred to a glass substrate.

FS-Galn fabrication

The LM-AgNW thin-film on the glass was sintered by the CW 532 nm laser source (Sprout-G-5W, Lighthouse Photonics) with a Galvano-mirror (hurrySCAN II, Scanlab). Optimal laser power range (1.0 W \sim 1.5 W) and laser scanning speed (100 mm s⁻¹) for FS-Galn sintering were found by the parametric study. After sintering was complete, the thin-film was placed in 0.2 M NaOH solution for 10 min for separation. The separated FS-Galn in the base solution was delicately held by tweezers and moved to an ethanol solution to eliminate the peripheral base solution. And then, the cleaned FS-Galn was dredged from the ethanol solution before (or after) applied to a target surface, and dried in an oven at 60 °C for 1 min.

FS-Galn sensor fabrication

FS-Galn sensor was made by laying FS-Galn over an index finger and contacting copper tape. It was encapsulated by VHB tape and the sensor signal was obtained.

Imaging and characterization

The digital images were taken by a smartphone (Galaxy S20, Samsung Electronics). An optical microscope (BX53M, Olympus) with Stream Basic software (version 2.2, Olympus) was utilized for high magnification optical images. SEM images were obtained from

a field-emission scanning electronic microscopy (AURIGA, Carl Zeiss). Elemental composition and mapping images were acquired using energy dispersive X-ray spectroscopy (Flat-Quad, Bruker) equipped in the field-emission scanning electronic microscopy.

Electromechanical performance measurements

To quantify the electromechanical characterization, a rectangular sample (length 10 mm \times width 0.5 mm) was prepared for the test. Initial conductivity of the FS-Galn was calculated as 5.79×10^5 S m⁻¹ from the conductivity equation $\sigma = l/Rwt$, where l , R , w , and t are length, resistance, width and thickness of FS-Galn sample, respectively. After laying the FS-Galn on VHB(3 M), a copper tape connected with an alligator clip was attached to the sample. To ensure the stability of contact between the FS-Galn and the copper tape, a small amount of EGaln was spread thinly on them. The sample was stretched from the initial gap of 3 mm with a uniform speed of 0.5 mm s⁻¹ through a uniaxial tensile load system (Physik Instrumente). Real-time electrical resistance was measured by the PXIE hardware system with LabVIEW software. (National Instrument).

The durability of the FS-Galn was measured under 100% mechanical strain with the same measuring instrument until 10,000 cycles. To investigate contact with a rigid component, a zero-ohm resistor bridged two FS-Galn, where they had a gap of 1 mm. The resistor was softly pressed to ensure stable contact when the resistor connected between the two FS-Galn lines. The electromechanical characteristic was measured in the same way; the sample was stretched with a uniform speed of 0.5 mm s⁻¹ through a uniaxial tensile load system until failure. To verify the electromechanical behavior of the repaired circuit, a circular FS-Galn repair patch was prepared in advance. The prepared patch simply covered the target area, which was intentionally created by erasing the previously existing FS-Galn circuit line by scrubbing with NaOH solution-soaked tissue. The electromechanical performance was measured in the same manner as the preceding measure procedure.

All electromechanical performance evaluations were conducted without any encapsulation.

DATA AVAILABILITY

The data that support the findings of this study are available from the corresponding author upon request.

Received: 7 August 2022; Accepted: 8 December 2022;

Published online: 26 December 2022

REFERENCES

- Kim, D. H. et al. Epidermal electronics. *Science* **333**, 838–843 (2011).
- Wang, R. et al. A Bi-Sheath Fiber Sensor for Giant Tensile and Torsional Displacements. *Adv. Funct. Mater.* **27**, 1702134 (2017).
- Zhu, Z. et al. Buckled Amorphous Hollow Carbon Spheres: Facile Fabrication, Buckling Process, and Applications as Electrode Materials for Supercapacitors. *ACS Appl. Mater. Interfaces* **11**, 30116–30124 (2019).
- Wen-Qian, H., Xiang, Z. & Zun-Feng, L. Recent progress on stretchable conductors. *Acta Phys. Sin.* **69**, 177401 (2020).
- Khodagholy, D. et al. NeuroGrid: recording action potentials from the surface of the brain. *Nat. Neurosci.* **18**, 310–315 (2015).
- Matsuhisa, N. et al. High-frequency and intrinsically stretchable polymer diodes. *Nature* **600**, 246–252 (2021).
- Li, W. L. et al. An on-demand plant-based actuator created using conformable electrodes. *Nat. Electron.* **4**, 134–142 (2021).
- Lu, H. et al. Reversible Underwater Adhesion for Soft Robotic Feet by Leveraging Electrochemically Tunable Liquid Metal Interfaces. *ACS Appl. Mater. Interfaces* **13**, 37904–37914 (2021).
- Thrasher, C. J., Farrell, Z. J., Morris, N. J., Willey, C. L. & Tabor, C. E. Mechanoresponsive Polymerized Liquid Metal Networks. *Adv. Mater.* **31**, 1903864 (2019).

10. Wang, Y. et al. A highly stretchable, transparent, and conductive polymer. *Sci. Adv.* **3**, 1602076 (2017).
11. Cao, Y. et al. A Transparent, Self-Healing, Highly Stretchable Ionic Conductor. *Adv. Mater.* **29**, 1605099 (2017).
12. Kim, K. K. et al. Highly Sensitive and Stretchable Multidimensional Strain Sensor with Prestrained Anisotropic Metal Nanowire Percolation Networks. *Nano Lett.* **15**, 5240–5247 (2015).
13. Won, P., Jeong, S., Majidi, C. & Ko, S. H. Recent advances in liquid-metal-based wearable electronics and materials. *iScience* **24**, 102698 (2021).
14. Tavakoli, M. et al. EGaln-Assisted Room-Temperature Sintering of Silver Nanoparticles for Stretchable, Inkjet-Printed, Thin-Film Electronics. *Adv. Mater.* **30**, 1801852 (2018).
15. Liu, S., Shah, D. S. & Kramer-Bottiglio, R. Highly stretchable multilayer electronic circuits using biphasic gallium-indium. *Nat. Mater.* **20**, 851–858 (2021).
16. Choi, J. et al. Customizable, conformal, and stretchable 3D electronics via pre-distorted pattern generation and thermoforming. *Sci. Adv.* **7**, abj0694 (2021).
17. Johnston, L., Yang, J., Han, J., Kalantar-Zadeh, K. & Tang, J. Intermetallic wetting enabled high resolution liquid metal patterning for 3D and flexible electronics. *J. Mater. Chem. C* **10**, 921–931 (2022).
18. Kim, M. S. et al. Stretchable Printed Circuit Board Based on Leak-Free Liquid Metal Interconnection and Local Strain Control. *ACS Appl. Mater. Interfaces* **14**, 1826–1837 (2022).
19. Xu, C. T., Ma, B., Yuan, S., Zhao, C. & Liu, H. High-Resolution Patterning of Liquid Metal on Hydrogel for Flexible, Stretchable, and Self-Healing Electronics. *Adv. Electron. Mater.* **6**, 1900721 (2020).
20. Liu, S., Reed, S. N., Higgins, M. J., Titus, M. S. & Kramer-Bottiglio, R. Oxide rupture-induced conductivity in liquid metal nanoparticles by laser and thermal sintering. *Nanoscale* **11**, 17615–17629 (2019).
21. Han, S. et al. Fast plasmonic laser nanowelding for a Cu-nanowire percolation network for flexible transparent conductors and stretchable electronics. *Adv. Mater.* **26**, 5808–5814 (2014).
22. Cho, C. et al. Monolithically Programmed Stretchable Conductor by Laser-Induced Entanglement of Liquid Metal and Metallic Nanowire Backbone. *Small* **18**, 2202841 (2022).
23. Kumar, S. & Singh, R. Nanofunctional gallium oxide (Ga₂O₃) nanowires/nanostructures and their applications in nanodevices. *psr RRL* **7**, 781–792 (2013).
24. Lopes, P. A. et al. Bi-Phasic Ag-In-Ga-Embedded Elastomer Inks for Digitally Printed, Ultra-Stretchable, Multi-layer Electronics. *ACS Appl. Mater. Interfaces* **13**, 14552–14561 (2021).
25. Park, J. E., Kang, H. S., Koo, M. & Park, C. Autonomous Surface Reconciliation of a Liquid-Metal Conductor Micropatterned on a Deformable Hydrogel. *Adv. Mater.* **32**, 2002178 (2020).
26. Zolfaghari, N., Khandagale, P., Ford, M. J., Dayal, K. & Majidi, C. Network topologies dictate electromechanical coupling in liquid metal-elastomer composites. *Soft Matter* **16**, 8818–8825 (2020).
27. Krisnadi, F. et al. Directed Assembly of Liquid Metal-Elastomer Conductors for Stretchable and Self-Healing Electronics. *Adv. Mater.* **32**, 2001642 (2020).
28. Lee, J. H., Lee, P., Lee, D., Lee, S. S. & Ko, S. H. Large-Scale Synthesis and Characterization of Very Long Silver Nanowires via Successive Multistep Growth. *Cryst. Growth Des.* **12**, 5598–5605 (2012).
29. Hao, X. P. et al. Self-Shaping Soft Electronics Based on Patterned Hydrogel with Stencil-Printed Liquid Metal. *Adv. Funct. Mater.* **31**, 2105481 (2021).
30. Hirsch, A., Michaud, H. O., Gerratt, A. P., de Mulatier, S. & Lacour, S. P. Intrinsically Stretchable Biphasic (Solid-Liquid) Thin Metal Films. *Adv. Mater.* **28**, 4507–4512 (2016).
31. Wang, J. et al. Printable Superelastic Conductors with Extreme Stretchability and Robust Cycling Endurance Enabled by Liquid-Metal Particles. *Adv. Mater.* **30**, 1706157 (2018).
32. Yan, Q. M., Zhou, M. & Fu, H. Q. A reversible and highly conductive adhesive: towards self-healing and recyclable flexible electronics. *J. Mater. Chem. C* **8**, 7772–7785 (2020).
33. Jung, D. et al. Highly conductive and elastic nanomembrane for skin electronics. *Science* **373**, 1022–1026 (2021).
34. Ding, C. et al. Omnidirectionally stretchable electrodes based on wrinkled silver nanowires through the shrinkage of electrospun polymer fibers. *J. Mater. Chem. C* **8**, 16798–16807 (2020).
35. Hubertus, J. et al. Nanoscale Nickel-Based Thin Films as Highly Conductive Electrodes for Dielectric Elastomer Applications with Extremely High Stretchability up to 200%. *ACS Appl. Mater. Interfaces* **13**, 39894–39904 (2021).

ACKNOWLEDGEMENTS

This work was supported by the National Research Foundation of Korea (grant number 2021R1A2B5B03001691, 2021M3H4A1A02050237).

AUTHOR CONTRIBUTIONS

M.K. and C.C. contributed equally to this work. M.K., C.C., and S.H.K. conceived and initiated the study. M.K. designed and performed the experiments. M.K. and C.C. analyzed the data. S.H.K. supervised the research program. J.K., J.J.P., W.S., and S.H.K. advised on the development of the idea. All authors discussed the results and wrote the paper.

COMPETING INTERESTS

The authors declare no competing interests.

ADDITIONAL INFORMATION

Supplementary information The online version contains supplementary material available at <https://doi.org/10.1038/s41528-022-00232-1>.

Correspondence and requests for materials should be addressed to Carmel Majidi or Seung Hwan Ko.

Reprints and permission information is available at <http://www.nature.com/reprints>

Publisher's note Springer Nature remains neutral with regard to jurisdictional claims in published maps and institutional affiliations.



Open Access This article is licensed under a Creative Commons Attribution 4.0 International License, which permits use, sharing, adaptation, distribution and reproduction in any medium or format, as long as you give appropriate credit to the original author(s) and the source, provide a link to the Creative Commons license, and indicate if changes were made. The images or other third party material in this article are included in the article's Creative Commons license, unless indicated otherwise in a credit line to the material. If material is not included in the article's Creative Commons license and your intended use is not permitted by statutory regulation or exceeds the permitted use, you will need to obtain permission directly from the copyright holder. To view a copy of this license, visit <http://creativecommons.org/licenses/by/4.0/>.

© The Author(s) 2022